

Spatial Interpolation of consolidation properties of Holocene clays at Kobe Airport using an artificial neural network

Kazuhiro Oda¹, Minsun Lee¹ and Shotaro Kitamura¹
¹Graduate School of Engineering, Osaka University, Japan

ABSTRACT: The spatial distribution of the consolidation properties for a seabed must be appropriately estimated to accurately predict the consolidation settlement due to large-scale reclamation. The soil properties must be estimated at arbitrary positions in the ground from data collected during soil investigation. In this study, an artificial neural network was applied to spatially interpolate consolidation properties such as the natural water content, void ratio, plastic index, compression index, and pre-consolidation pressure. The estimation accuracy of consolidation properties was judged based on four indexes: R2, G, MARE, and SR. The artificial neural network estimated the appropriate consolidation properties with high accuracy; this confirmed the availability of spatial interpolation of consolidation properties by using an artificial neural network.

Keywords: Neural Network, Geoinformatics, Spatial Interpolation, Holocene Clay, Soil Properties

1. INTRODUCTION

Many manmade islands have been built in Osaka Bay, such as Kansai International Airport, Port Island, and Yumeshima Island. In addition, the construction of new manmade islands is presently in the planning stage. Manmade islands are usually constructed for the long term because they are very large. During construction of manmade islands, they are usually divided into sections. The construction histories are different for each section, which means differential settlement of the manmade islands occurs. Therefore, the differential settlement must be predicted to manage the construction of manmade islands.

Holocene clays more than 20 m in depth have accumulated in Osaka Bay under almost normally consolidated conditions. The differential settlement of manmade islands in Osaka Bay mainly depends on the consolidation behavior of the Holocene clay layer. The spatial distribution of consolidation properties such as the compression index and coefficient of permeability in the Holocene clay layer must be elucidated to accurately predict the differential settlement of manmade islands. However, it is difficult to estimate the spatial distribution of consolidation properties from a limited number of soil investigations.

An artificial neural network is an information processing system that has been developed recently. This technique is applied to data mining. Data mining is the process of discovering new patterns from a large number of datasets. In other words, locations at which soil investigations were carried out and geotechnical information obtained from soil investigations can be chosen as datasets. The connection between the locations at soil investigations and geotechnical information can be given by applying an artificial neural network. The authors previously studied the spatial interpolation of soil properties by using an artificial neural network [1]-[3]. An artificial neural network was applied to estimate the soil properties at an arbitrary

position in the ground. In other words, the spatial interpolation of soil properties was carried out by using an artificial neural network.

In this study, the spatial distribution of consolidation properties, which are used to predict the differential settlement of manmade islands, was carried out by using an artificial neural network. In other words, an artificial neural network was applied to estimate the consolidation properties at arbitrary positions in the Holocene clay layer. The estimation accuracy of the consolidation properties was judged through various statistical indexes. The spatial distribution of consolidation properties in the Holocene clay layer was visualized. The availability of an artificial neural network for spatial interpolation of consolidation properties was examined based on the accuracy of the results.

2. ARTIFICAIL NEURAL NETWORK

An artificial neural network is an information processing system, in which the nerve cells (neurons) of the human brain are reproduced mathematically. Fig. 1 shows the architecture of the artificial neural network used in this study. This type of artificial neural network is called a back propagation neural network; it is the most popular neural network in use. The back propagation neural network consists of an input layer, one or more hidden layers, and the output layer. Each layer is connected by neurons. In this study, the consolidation properties at an arbitrary position in the ground were estimated. Then, the latitude, longitude, and altitude at a target position at which the consolidation properties were estimated were correlated to items of the input layer. The consolidation pressures obtained through oedometer tests were added to items of the input layer, if one-dimensional compression curves were estimated. Estimated soil properties were correlated to items of the output layer.

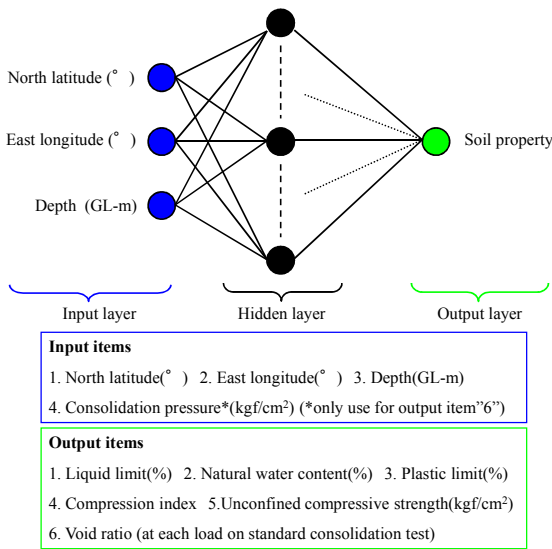


Fig. 1. Architecture of artificial neural network

3. ANALYSIS

3.1 Subject Area for Spatial Interpolation

Large amounts of geotechnical information have been obtained from soil investigations of many construction projects in the Kansai area; this information has been collected into a geoinformatics database called Gbase [4]. Fig. 2(a) shows the locations of soil investigations included in Gbase. The red dots denote the locations at which soil investigations were carried out. Over 25,000 boring investigations in the Kansai area have been carried out, and the data are accumulated into Gbase. In this study, the spatial interpolation of consolidation properties in Holocene clay (Ma13) at Kobe Airport in Osaka Bay was carried out. Fig. 2(b) shows the locations of soil investigations in the subject area of this study. Ninety-nine boring investigations were applied to determine the optimum architecture of the artificial neural network.

3.2 Analysis Procedure

The architecture of an artificial neural network must be determined to optimally estimate the consolidation properties at an arbitrary position in the ground. The process of determining the architecture is called “training.”

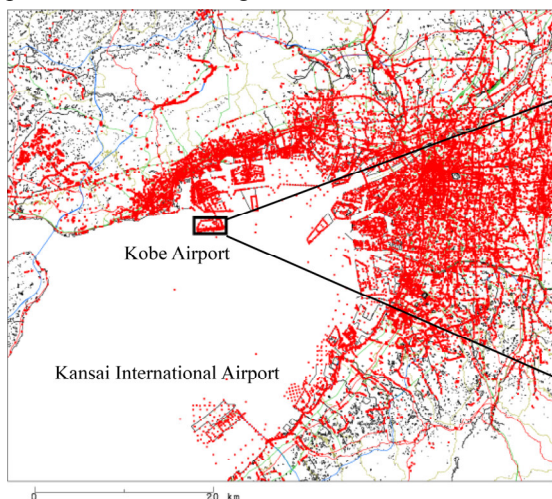


Fig. 2(a). Locations of soil investigations in Gbase.

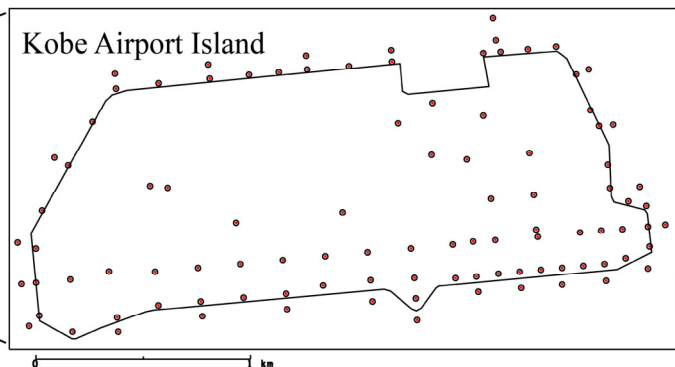


Fig. 2(b) Locations of boring investigations in subject area

A large number of pairs of input and output items are required in the training process. An artificial neural network is trained as follows. First, the initial network has randomly assigned weights. When input data are given to the input layer of this network, they are propagated through the hidden layer to the output layer; after this, output data can be obtained. However, there are differences between the estimated output values and real values. The network and weights are updated automatically to minimize the errors. Training is repeated until the repetition reaches a preliminarily given number. The optimal network structure is determined in this manner.

3.3 Indexes for Judging Optimum Architecture

Four indexes were used to choose the optimum architecture of an artificial neural network: R^2 , G , $MARE$ and SR .

R^2 (coefficient of correlation) is popularly used in statistics for obtaining a linear regression between the estimated value and a target value. It is defined as follows:

$$R^2 = \frac{\frac{1}{N} \sum_{i=1}^N (x_i^o - \bar{x}^o)(x_i^p - \bar{x}^p)}{\sqrt{\frac{1}{N} \sum_{i=1}^N (x_i^o - \bar{x}^o)^2} \sqrt{\frac{1}{N} \sum_{i=1}^N (x_i^p - \bar{x}^p)^2}} \quad (1)$$

where N is the number of pairs of samples, x_i is the value of each sample, and \bar{x} is the mean value of the samples. Superscripts o and p denote the estimated and target values, respectively.

G (prediction accuracy) is defined as follows [5]:

$$G = \left(1 - \frac{RMSE}{RMS}\right) \times 100 \quad (2)$$

where $RMSE$ (root-mean-squared error) and RMS (root mean squared) are respectively defined as follows:

$$RMSE = \sqrt{\frac{1}{N} \sum_{i=1}^N (x_i^p - x_i^o)^2} \quad (3)$$

$$RMS = \sqrt{\frac{1}{N} \sum_{i=1}^N x_i^{o2}} \quad (4)$$

The higher the estimation accuracy is, the higher both R^2 and G is. $MARE$ (mean absolute relative error) is defined as follows:

$$MARE = \frac{1}{N} \sum_{i=1}^N |x_i^p - x_i^o| \quad (5)$$

The higher the estimation accuracy is, the lower $MARE$ is. In addition, both G and $MARE$ are indexes to judge the estimation accuracy of a set of estimated values. SR (success rate) is used to judge the accuracy of each estimated value. It is based on the absolute error r at each estimated value. r_i is defined as follows:

$$r_i = \frac{|x_i^p - x_i^o|}{x_i^o} \quad (6)$$

In this study, three different ranges of SR (%) were used to judge the estimation accuracy: $r_i < 10\%$, r_i between 10% and 15%, and $r_i > 15\%$ [6].

4. ESTIMATION ACCURACY

4.1 Natural Water Content

Table 1 shows the estimation accuracy of the natural water content. In each case, R^2 was over 0.9, G was almost 80%, and $MARE$ was less than 12%. Thus, the natural water content can be estimated by the artificial neural network. In particular, WN-1 had the highest G and lowest $MARE$. In addition, WN-1 had the highest SR when $r < 10\%$. WN-1 had the highest estimation accuracy among the four cases. The artificial neural network could reproduce the distribution of the natural water content.

Fig. 3 shows the three-dimensional distribution of natural water content. The natural water content in Fig. 3 was estimated using WN-1. First, the subject area was divided

into about 67,000 regions. Second, the latitude, longitude, and altitude of each region were calculated. Finally, the natural water content in each region was estimated by applying the latitude, longitude, and altitude to the WN-1 artificial neural network. Fig. 3 clearly shows the distribution of natural water content. The natural water content decreased in the east-to-west direction. The natural water content was highest in the southeast corner of the seabed surface of the subject area at over 100%. The natural water content was about 90% at the northwest corner of the seabed surface in the subject area. The natural water content decreased with increasing depth. The natural water content in the bottom layer of Holocene clay was about 50%. The natural water content showed almost no change in the north-to-south direction.

4.2 Void Ratio

Table 2 shows the estimation accuracy of the void ratio. In each case, R^2 was over 0.9, G was more than 93%, and $MARE$ was only slightly over 5%; thus, the void ratio can be estimated by the artificial neural network. The VR-3 artificial neural network produced the most accurate estimations among the four cases judging from SR .

Fig. 4 shows the three-dimensional distribution of the void ratio. The void ratio in Fig. 4 was estimated by using the

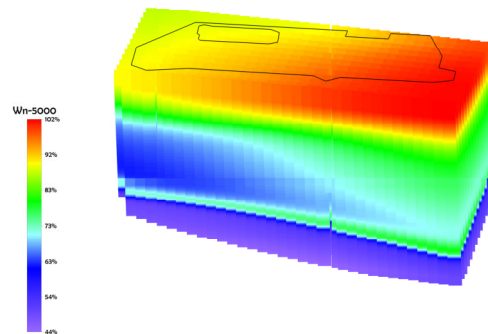


Fig. 3. Three-dimensional distribution of natural water content (WN-1)

Table 1. Estimation accuracy of natural water content

Case	Repetition Number	R^2	G (%)	$MARE$ (%)	SR (%)		
					$r < 10$	$10 < r < 15$	$r > 15$
WN-1	5000	0.934	87.10	11.56	80.9	6.6	12.6
WN-2	10000	0.935	87.13	11.63	79.9	6.8	13.3
WN-3	15000	0.936	87.15	11.60	80.7	7.2	12.2
WN-4	20000	0.936	87.16	11.58	79.3	8.9	11.8

Table 2. Estimation accuracy of void ratio

Case	Repetition Number	R^2	G (%)	$MARE$ (%)	SR (%)		
					$r < 10$	$10 < r < 15$	$r > 15$
VR-1	5000	0.912	93.46	5.29	89.2	6.7	4.1
VR-2	10000	0.911	93.36	5.21	90.2	5.7	4.1
VR-3	15000	0.908	93.16	5.45	88.1	6.2	5.7
VR-4	20000	0.911	93.49	5.20	88.7	7.2	4.1

VR-3 artificial neural network. The same method of estimating the natural water content was applied to obtain Fig. 4. The void ratio decreased in the east-to-west direction. The void ratio was highest at the southeast corner of the seabed surface in the subject area, at about 3.0. It was about 2.5 at the northwest corner. The void ratio decreases with increasing depth. The void ratio in the bottom layer of Holocene clay was about 1.5. The void ratio hardly changed in the north-to-south direction.

The distribution of the void ratio corresponded to that of the natural water content, as shown in Fig. 3. The Holocene clay layer on the east side of Kobe Airport was thicker than on the west side. Moreover, both the natural water content and void ratio on the east side of the airport were higher than on the west. The settlement during construction on the east side was predicted to be larger than that on the west side. The construction work on Kobe Airport was carried out in consideration of the differential settlement.

4.3 Plastic Index

Table 3 shows the estimation accuracy of the plastic index. In each case, R^2 was almost 0.94, G was almost 90%, and $MARE$ was about 8%; thus, the plastic index can be estimated with the artificial neural network.

Fig. 5 shows the three-dimensional distribution of the

plastic index. The plastic index was estimated by the IP-1 artificial neural network. The same method of estimating the natural water content and void ratio was applied to make Fig. 5. The plastic index decreased in the east-to-west direction in the same manner as the natural water content and void ratio. The plastic index was highest at the southeast corner of the seabed surface in the subject area. The plastic index was lowest at the northwest corner. The plastic index decreased with increasing depth. The variation in the plastic index around both the surface and bottom was significant. The void ratio hardly varied in the north-to-south direction.

4.4 Compression Index

Table 4 shows the estimation accuracy of the compression index. In each case, R^2 was over 0.8. This value was lower than the values for the natural water content, void ratio, and plastic index. G was almost 87%, and $MARE$ was almost 10%. The estimation accuracy for the compression index was slightly lower than the estimation accuracies for the natural water content, void ratio, and plastic index. The CC-3 artificial neural network had the most accurate estimates among the four cases, judging from all four indexes.

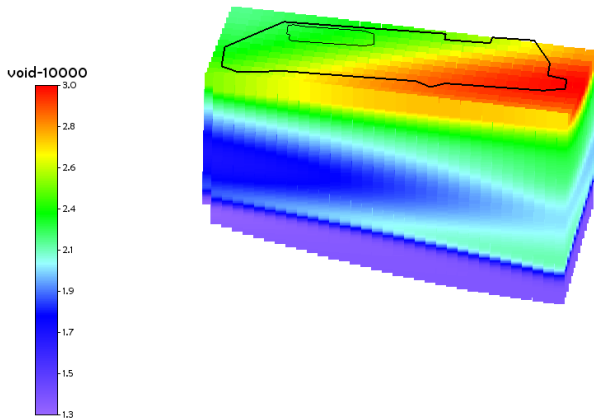


Fig. 4. Three-dimensional distribution of void ratio (VR-3)

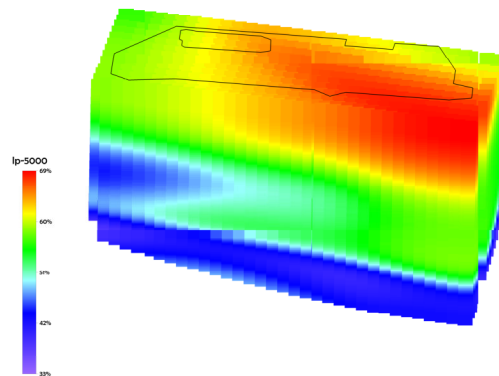


Fig. 5. Three-dimensional distribution of plastic index (IP-1)

Table 3. Estimation accuracy in plastic index

Case	Repetition Number	R^2	G (%)	$MARE$ (%)	SR (%)		
					$r < 10$	$10 < r < 15$	$r > 15$
IP-1	5000	0.934	90.31	7.67	72.3	12.3	15.4
IP-2	10000	0.935	89.84	7.78	68.7	14.4	16.9
IP-3	15000	0.936	89.61	8.09	71.3	12.3	16.4
IP-4	20000	0.936	90.12	7.79	72.8	11.3	15.9

Table 4. Estimation accuracy (compression index)

Case	Repetition Number	R^2	G (%)	$MARE$ (%)	SR (%)		
					$r < 10$	$10 < r < 15$	$r > 15$
CI-1	5000	0.832	87.10	10.48	60.3	20.6	19.1
CI-2	10000	0.852	87.80	10.23	67.0	16.0	17.0
CI-3	15000	0.848	87.55	10.44	62.9	17.5	19.6
CI-4	20000	0.813	86.49	11.09	63.9	19.1	17.0

Fig. 6 shows the three-dimensional distribution of the compression index. The compression index in Fig. 6 was estimated by the CC-2 artificial neural network. The same method for estimating the other soil properties was applied to obtain Fig. 6. The compression index for the upper and middle parts of the Holocene clay layer was almost 0.9. It slightly decreased in the east-to-west direction. However, the variation was extremely small. The compression index of the lower part increased with depth. It decreases significantly in the bottom part of the Holocene clay layer. The maximum compression index was greater in the lower part of the east side of the subject area. This index decreased in the east-to-west direction.

4.5 Pre-Consolidation Pressure

Table 5 shows the estimation accuracy of the pre-consolidation pressure. In each case, R^2 was over 0.95, G was more than 87%, and MARE was almost 12%. However, SR when $r < 10\%$ was about 53%–61%, and SR when $r > 15\%$ was about 24%–27%. This implies that the estimated values with errors of less than 10% made up about 53%–61% of the total, and that with errors greater than 15% made up about 24%–27% of the total. The PC-4

artificial neural network had the most accurate estimates of the four cases judging from SR .

Fig. 7 shows the three-dimensional distribution of the pre-consolidation pressure. The pre-consolidation pressure in Fig. 7 was estimated by the PC-4 artificial neural network. The same method for estimating the other soil properties was applied to obtain Fig. 7. The pre-consolidation pressure increased with depth. There was hardly any distinguishing spatial variation in the subject area.

4.6 One-Dimensional Compression Curve

One-dimensional compression curve is obtained from consolidation pressure and void ratio. The item of consolidation pressure must be added to input layer in Fig. 1. Table 6 shows the estimation accuracy of one-dimensional compression curve. In each case, quite high accuracy could be obtained; R^2 is over 0.95, G is over 90%, and $MARE$ is less than 5%. Also, SR in $r < 10$ is higher than almost 90%.

Fig. 8 shows the examples of estimated one-dimensional consolidation curves. The agreement between the target value and estimated value is good. Especially, the estimated

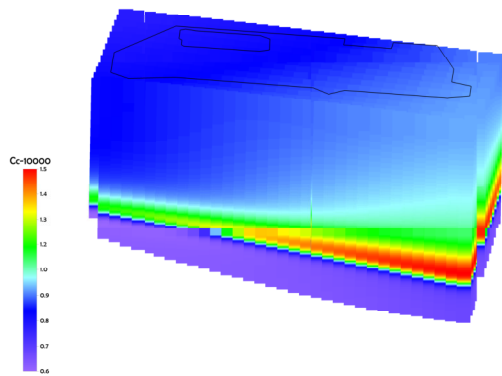


Fig. 6. Three-dimensional distribution of compression index (CC -2)

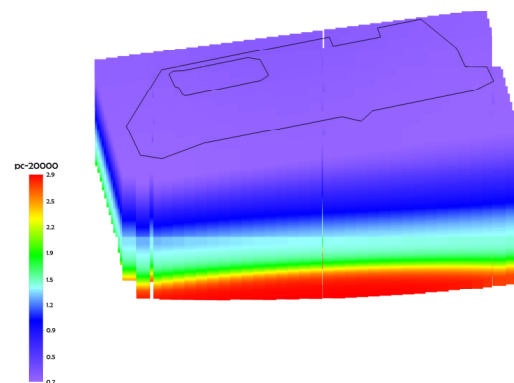


Fig. 7. Three-dimensional distribution of pre-consolidation pressure (PC-1)

Table 5. Estimation accuracy (pre-consolidation pressure)

Case	Repetition Number	R^2	G (%)	$MARE$ (%)	SR (%)		
					$r < 10$	$10 < r < 15$	$r > 15$
PC-1	5000	0.963	87.33	12.74	52.6	20.1	27.3
PC-2	10000	0.964	87.67	12.35	53.6	20.1	26.3
PC-3	15000	0.962	87.38	12.21	56.2	19.1	24.7
PC-4	20000	0.964	87.66	12.06	60.8	14.9	24.2

Table 6. Estimation accuracy (One-dimensional compression curve)

Case	Repetition Number	R^2	G (%)	$MARE$ (%)	SR (%)		
					$r < 10$	$10 < r < 15$	$r > 15$
OC-1	5000	0.961	93.81	4.84	88.54	7.45	4.02
OC-2	10000	0.966	94.23	4.61	91.72	5.36	2.93
OC-3	15000	0.965	94.11	4.72	89.37	7.03	3.60
OC-4	20000	0.966	94.23	4.58	90.04	6.19	3.77

Table 7. Estimation accuracy (Permeability vs. void ratio)

Case	Repetition Number	R^2	G (%)	$MARE$ (%)	SR (%)		
					$r < 10$	$10 < r < 15$	$r > 15$
PV1	5000	0.934	86.26	12.88	52.38	19.33	28.28
PV-2	10000	0.935	86.27	12.68	54.48	17.32	28.20
PV-3	15000	0.936	86.41	12.44	56.57	15.98	27.45
PV-4	20000	0.936	86.46	12.72	55.06	15.82	29.12

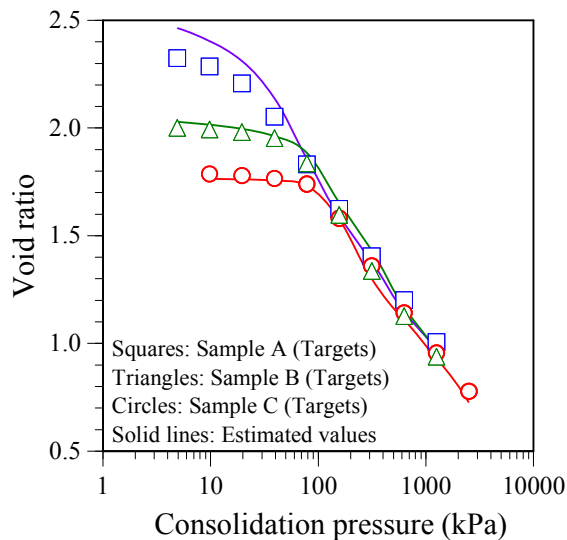


Fig. 8. Examples of estimated one-dimensional compression curves (OC-2)

values in Sample B (green solid line) and Sample C (red solid line) are closely coincident with the target values in Sample B (green triangles) and Sample C (red circles). Also, the one-dimensional compression curve, relationship between the logarithmic of consolidation pressure and void ratio, in Fig. 8 almost match under normally consolidated, because these samples are taken from same boring investigation.

4.7 Permeability

Permeability is calculated from coefficient of consolidation and coefficient of volume compressibility, which are getting each loading step in oedometer test. Table 7 shows the estimation accuracy of relationship between permeability and void ratio. In each case, R^2 was over 0.93, G was more than 86%, and $MARE$ was almost 13%. However, SR when $r < 10\%$ was about 52%–57%, and SR when $r > 15\%$ was over 27%. This implies that the estimated values with errors of less than 10% made up about 52%–57% of the total, and that with errors greater than 15% made up about 27% of the total. It is necessary to improve the estimation method for permeability.

5 CONCLUSION

Spatial interpolation of consolidation properties in Holocene clay at Kobe Airport was carried out using an artificial neural network. The main conclusions are summarized as follows:

1. An artificial neural network can be applied to estimate the consolidation properties at arbitrary positions in the

Holocene clay layer of Osaka Bay.

2. The artificial neural network estimated the consolidation properties with high accuracy. In particular, the estimation accuracy for the natural water content, void ratio, plastic index and one-dimensional compression curve was excellent.
3. The spatial interpolation of consolidation properties could be carried out with an artificial neural network.
4. Not only physical properties but also mechanical behavior of clays, such as one-dimensional compression curve can be estimated through artificial neural network.
5. The consolidation properties interpolated spatially could be visualized three-dimensionally, so it was very easy to recognize the distribution of consolidation properties.

6 REFERENCES

- [1] Oda, K, Ikeda, S, and Tokida, K, "Spatial interpolation of soil properties in Osaka Bay area through artificial neural network," Proc Symposium on Geoinformatics and Zoning for Hazard Mapping, 2009, pp. 178-181.
- [2] Oda, K, "Spatial interpolation of soil properties in north area of Osaka Bay through artificial neural network," Advances in Ground Technology & Geo-Information, 2011, pp. 143-150.
- [3] Oda, K, Kitamura, S, and Lee, MS, "Applicability of artificial neural network to spatial interpolation of soil properties in Kansai International Airport," Proceedings of the Twenty-Second (2012) International Offshore and Polar Engineering Conference, 2012, pp. 583-586.
- [4] Tanaka, Y, and Tsukada, Y, "Geotechnical database of Kansai - history and developments," Proc Symposium on Geoinformatics and Zoning for Hazard Mapping, 2009, pp. 85-92.
- [5] Juang, CH, Jiang, T, and Christopher, RA, "Three-dimensional site characterization: neural network approach," Geotechnique, Vol. 51, No. 9, 2001, pp. 799-809.
- [6] Erdal, U, Mustafa, L, Ahmet, S, and Bekir, KH, "Prediction of lateral effective stresses in sand using artificial neural network," Soils & Foundations, Vol. 48, No. 2, 2008, pp. 141-153.

Int. J. of GEOMATE, March, 2013, Vol. 4, No. 1 (Sl. No. 7), pp.423-428

MS No. 232 received July 23, 2012, and reviewed under GEOMATE publication policies. Copyright © year, International Journal of GEOMATE. All rights reserved, including the making of copies unless permission is obtained from the copyright proprietors. Pertinent discussion including authors' closure, if any, will be published in the month, year if the discussion is received by Sept, 2013.

Corresponding Author: Kazuhiro Oda
